Dosimetric impact of respiratory motion during boron neutron capture therapy for lung cancer

Shaojuan Wu[a], Changran Geng[a], Xiaobin Tang[a,*], Silva Bortolussi[b,c], Yang Han[a], Diyun Shu[a], Chunhui Gong[a,c], Xinxin Zhang[a], Feng Tian[a]

[a] Department of Nuclear Science and Technology, Nanjing University of Aeronautics and Astronautics, Nanjing, China
[b] Department of Physics, University of Pavia, Pavia, Italy
[c] National Institute of Nuclear Physics (INFN), Pavia, Italy

ARTICLE INFO

ABSTRACT

Lung cancer is one of the cancers with high morbidity and mortality. Boron neutron capture therapy (BNCT) has attracted researchers' attention in recent years because of its unique advantages in lung cancer treatment. However, changes in dose distribution in BNCT due to respiratory motion have not been studied. In this work, the tumor dose deviation caused by respiration was quantitatively investigated. Four-dimensional Computed Tomography (4D CT) was used to construct the virtual respiratory patient model in this study. Six phases (e.g., 10%, 20%, 50%, 60%, 80%, and 90%) were selected to represent the anatomy of patients at different moments throughout the respiratory cycle. Tumor-related dose volume histograms (DVH) indices at different phases were calculated using Monte Carlo toolkit. The results showed that the dose difference increased with the increasing of respiratory motion amplitude. In the three movement directions of the tumor, the dose changes caused by the movement in the anterior–posterior (AP) direction were remarkable under the treatment planning configurations we studied. The differences of tumor mean dose ranged from −13.8% to 15.8%. Similar conclusions were observed in the cases of three real patients.

1. Introduction

Lung cancer has been the leading cause of cancer mortality, and its incidence is increasing worldwide. The treatment methods of lung cancer include surgery, chemotherapy and radiotherapy (Alvarado-Luna and Morales-Espinosa, 2016; Bray et al., 2018). Among these treatments, radiotherapy plays an increasingly important role in lung cancer treatment.

Boron neutron capture therapy (BNCT) is a binary cancer treatment based on the nuclear reaction ^{10}B (n, α) ^{7}Li. The products of this reaction have high linear energy transfer (LET) characteristics (α particle, E ~ 150 keVμm-1, 7Li ion, E ~ 175 keVμm-1). The path lengths of these particles are shorter than the mean cell diameter that allows cell-selective irradiation to damage the tumor while sparing the surrounding normal tissues (Moss, 2014). In recent years, scholars proposed the use of BNCT to treat lung cancer because of its significant superiority to conventional radiotherapies in principle. In 2006, the Kyoto University Research Team performed a dosimetric study to evaluate the feasibility of BNCT for malignant pleural mesothelioma, which verified that BNCT could be a promising treatment modality for

these patients. Two years later, they went on clinic to treat a patient with mesothelioma with good outcomes. Follow-up was performed eight months after treatment. The patient's chest pain disappeared without late side effects (Suzuki et al., 2012, 2006). In 2014, R. Farías from the Comisión Nacional de Energía Atómica collaborated with the oncology institute Roffo (University of Buenos Aires) and University of Pavia to further investigate the neutron source energy ranges for lung cancer treatment (Farías et al., 2014). These studies demonstrated the feasibility and effectiveness of BNCT for treating patients with lung cancer.

Studying the dosimetric effects of respiratory motion during treatment is always a hot topic in the era of precision radiotherapy. However, whether the respiratory motion have an effect on the dose distribution during BNCT treatment has not been studied. Therefore, this study aimed to comprehensively study the dosimetric impact of respiration in BNCT for lung cancer and to estimate the resulting dose differences to achieve more accurate predictions of the actual dose administered to patients.

---

* Corresponding author.
  E-mail address: tangxiaobin@nuaa.edu.cn (X. Tang).
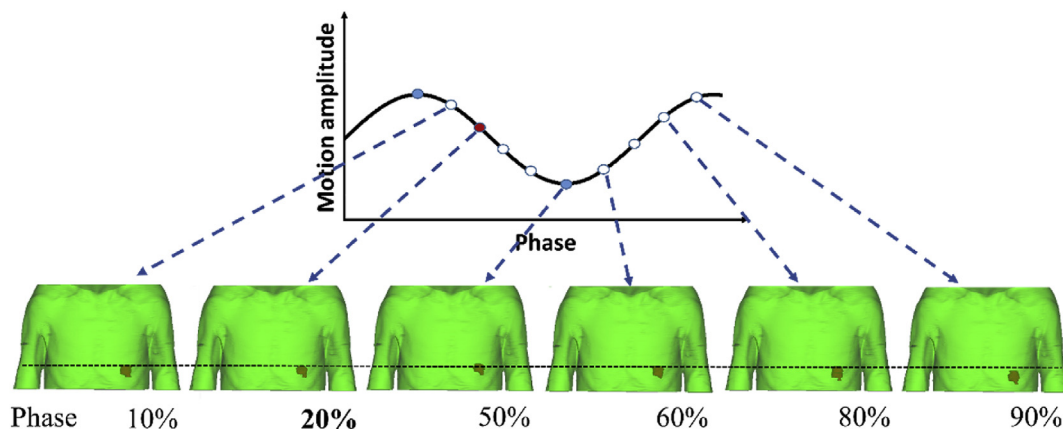
Fig. 1. Tumor location at the six phases. The green area represents the body, and the red area represents the tumor. (For interpretation of the references to colour in this figure legend, the reader is referred to the Web version of this article.)

2. Materials and methods

2.1. Construction of voxelized patient geometry

The patient geometry for dose calculation was constructed based on Four-dimensional computed tomography (4D CT) images of lung cancer patients. 4D CT is a dynamic image that comprises a series of three-dimensional images. It divides the breathing cycle into 10 phases (i.e., 0%, 10%, 20%, 30%, 40%, 50%, 60%, 70%, 80%, and 90%), and the CT images of each phase record the anatomy of the body at the corresponding moment (Eom et al., 2010; Yang et al., 2018).

Six phases, namely, 10%, 20%, 50%, 60%, 80%, and 90%, were used to represent the human body structure during the whole respiratory cycle (Fig. 1). Phase 20% was defined as the reference phase, because the tumor at this phase is in the middle of the respiratory motion. The dosimetric parameters of tumor in different phases were compared. The total tissue was divided into 24 materials based on the Schneider method, which converts the Hounsfield Unit (HU) value to material density and elemental composition (Schneider et al., 2000). The resolution of the reconstructed geometry is $1.95 \times 1.95 \times 2\,mm^3$. A C++ program was used to generate the binary file, which can be inputted to the Monte Carlo toolkit as the geometry model.

2.1.1. construction of a virtual respiratory patient model

A virtual respiratory patient model with moving tumor was established to explore the influence of respiratory motion on dose distribution. The motion trajectory in each direction was based on the study of George et al. (2005) and the ranges of respiratory motion in different directions obtained from Erridge (Erridge et al., 2003). The tumor's depth ranged from 1.5 cm to 4.9 cm.

The following formulas (George et al., 2005) were used to describe the spatial location of tumors at different phases,

$$x = bx \times \cos\frac{2\pi t}{\tau}, \tag{1}$$

$$y = by \times \cos\frac{2\pi t}{\tau}, \tag{2}$$

$$z = bz \times \cos\frac{2\pi t}{\tau}, \tag{3}$$

where t is the time parameter; and bx, by, and bz are the amplitudes of the tumor that moves in the lateral (LR), anterior–posterior (AP), and superior–inferior (SI) directions, respectively; and τ is the motion period (s).

The amplitudes of motion in the LR, AP, and SI directions were set as 3–13, 5–21, and 5–35 mm, respectively (Erridge et al., 2003). The range of motion was divided into 3, 8, and 13 mm in the LR direction; 5,

9, 13, 17, and 21 mm in AP direction; and 5, 12, 19, 26, and 34 mm in SI direction. The breathing period in this study was 5 s (i.e., τ was 5 s), which was also used in previous studies that assessed 4D radiotherapy (Grassberger et al., 2013; Knopf et al., 2011). We determined the tumor dose parameters by independently considering the respiratory motion in each direction (i.e., LR, AP, and SI). The deformation of the target structure during motion was not considered, indicating that the target was considered rigid during the breathing cycle (Schaefer et al., 2004).

2.1.2. construction of real patient geometry

Three real patient cases with different tumor motion amplitudes were investigated. Fig. 2 shows the transaxial, sagittal and coronal image slices through the tumor isocenter for each patient. The tumor of Patient I is located in the upper lobe of the right lung, with a tumor depth of 4–7.3 cm. The tumor of Patient II is located in the middle and lower lobes of the right lung with a tumor depth of 2.5–5.4 cm. For patient III, the tumor located at the lower lobe of the right lung, that is, at the junction of the right lung and liver. Table 1 shows the details about the tumor of each patient.

2.2. Treatment configurations

2.2.1. Neutron source

MIT-SPECT beam, which was based on the published energy spectrum of the MIT-II epithermal reactor beam developed for BNCT, was selected in this study (Kiger III et al., 1999) based on the conclusions
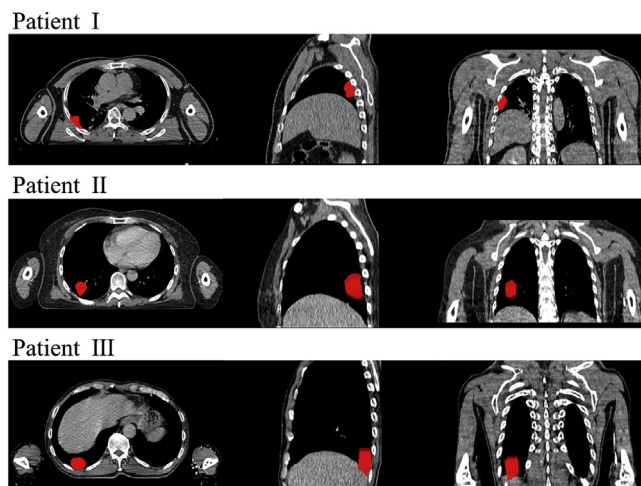
Fig. 2. CT image slices of the transaxial, sagittal, and coronal planes of the three patients.

Table 1
Tumor characteristics of Patients I, II, and III, including tumor motion amplitude, size, and depth.

Patient	Motion amplitudes (mm)			Tumor volume (cc)	Tumor depth (cm)
	SI	LR	AP		
I	< 2	/	/	13.57	4–7.3
II	10	3	1.5	13.16	2.5–5.4
III	16	3	2	13.38	2–4.2

Table 2
RBE and CBE factors used to convert the absorbed dose (Gy) into photon equivalent dose (Gy_w).

BNCT dose component	Normal tissues	Tumor	Skin
^{10}B (n,α)^{7}Li	1.4	3.8	2.5
^{14}N (n,p)^{14}C	3.2	3.2	3.2
Fast neutron	3.2	3.2	3.2
Photon	1	1	1

Table 3
Constraints of healthy organ dose for single-fraction SBRT of photon therapy.

	Threshold dose
Heart	[a]$D_{max} < 22$ Gy
Spinal cord	[a]$D_{max} < 14$ Gy
Skin	[a]$D_{max} < 26$ Gy
Lung	[b]$D_{mean} < 7.5$ Gy, [c]$V_5 < 26\%$
Liver	[d]$(V_0–V_{9.1}) > 700$ cc

[a] Maximum dose.
[b] Mean dose.
[c] Volume surrounded by the isodose curve of 5 Gy.
[d] Volume of liver with dose below 9.1 Gy.

drawn from the previous study (Yu et al., 2017). Fig. 3 shows that epithermal neutron beam with a 6 cm radius was used to perpendicularly irradiate the models. Source-skin distance was set to 5 cm. The center axis of the irradiation field was consistent with the tumor center of the 20% phase.

2.2.2. Boron concentration

To satisfy the therapeutic requirements of BNCT, a tumor-to-normal tissue boron concentration ratio, which was applied for the feasible treatments of BNCT from the viewpoint of dose distribution analysis, was set at 3.5 (González et al., 2004; Suzuki et al., 2006), the boron concentrations in the normal tissues, skin, and tumor were assumed as 10, 15 and 35 ppm respectively.

2.3. Dose calculation

The TOol for PArticle Simulation (TOPAS) (Perl et al., 2012), a Monte Carlo toolkit based on Geant4 (Agostinelli et al., 2003; Allison et al., 2006), was used in the dose calculation. TOPAS retains all the features of Geant4 in terms of speed, accuracy, and flexibility, providing a standardized basic physical database. The g4em-standard_opt4, thermalphp_physics, g4decay, g4ion-binarycascade, g4h-elastic_HP, g4stopping, g4em-extra and other physical processes were adopted in this simulation, as recommended by previous studies (Geng et al., 2015).

The BNCT dose can be divided into four parts. The dose that stem from the interaction of thermal neutrons with ^{10}B atoms in tissue through ^{10}B (n, α)^{7}Li reaction is called D_B. The dose that primarily arises from ^{14}N (n, p)^{14}C thermal neutron capture reaction is called D_{th}. Fast neutrons with energies above 10 keV that deliver the dose through elastic collisions with hydrogen nuclei in tissue via ^{1}H (n, n$_0$)^{1}H reaction, is called D_f. The dose component related to photons that can be generated from unavoidable gamma contamination of the beam and induced gamma dose in tissues is called D_γ.

Photon-equivalent dose H (Gy) is the photon equivalent dose of the BNCT dose. It was computed by multiplying each absorbed dose component by the relative biological effectiveness (RBE) and compound biological effectiveness (CBE) factors listed in Table 2 (Ishiyama, 2014), as follows:

$$H= W_B \times D_B + W_f \times D_f + W_{th} \times D_{th} + D_\gamma \qquad (4)$$

2.4. Dose evaluations and analysis

Dose volume histogram (DVH) indices for organs and the percentage difference values were used to evaluate and analyze the dose deviation of different phases. In this research, common criteria were selected to evaluate the treatment plans from Ettinger (Ettinger et al., 2017) and AAPM task group no.101 report (Benedict et al., 2010), which was similar to the previous study on BNCT treating lung cancer patients (Farías et al., 2014). Table 3 lists the dose constraints of healthy organs adopted to evaluate a treatment plan.

$$\text{percentage difference} = \frac{D_x - D_r}{D_r} * 100\%, \qquad (5)$$

where Dr represents the dose parameter in the reference phase, and Dx represents the dose parameter of other phases. Research attention should be given when the percentage difference is greater than 5% referred to ICRU Report 24, which pointed out that a 5% dose deviation in the target volume may lead to a recurrence of primary tumor and an increase in the probability of normal tissue complications (Leunens et al., 1992).
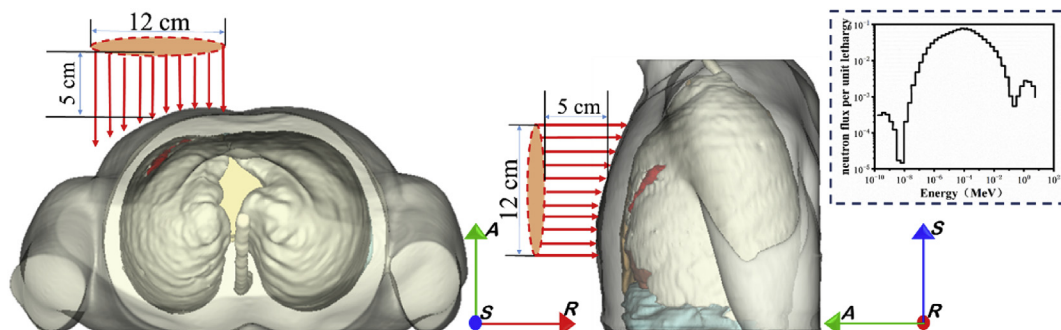
Fig. 3. Schematic diagram of geometry and beam settings for patients treated with BNCT (the red area represents the tumor). The top right corner shows the MIT-SPECT neutron spectrum. (For interpretation of the references to colour in this figure legend, the reader is referred to the Web version of this article.)

Table 4
Percentage differences of mean dose and $D_{95\%}$ at different phases in the range of 3–13 mm in LR motion.

Phase	Dose	Tumor dose differences (%) at each phase of different motion amplitudes in the LR direction		
		3 mm	8 mm	13 mm
10%	D_{mean}	−0.4	−0.4	0.2
	$D_{95\%}$	−0.6	−0.7	0.4
20%	D_{mean}	–	–	–
	$D_{95\%}$	–	–	–
50%	D_{mean}	−0.1	−0.8	−1.6
	$D_{95\%}$	−1.1	−1.9	−3.3
60%	D_{mean}	0.1	−0.7	−1.5
	$D_{95\%}$	−0.7	−1.7	−3.0
80%	D_{mean}	0.1	0.7	0.7
	$D_{95\%}$	0.4	1.1	1.1
90%	D_{mean}	0.1	0.1	0.6
	$D_{95\%}$	0.7	0.7	1.3

3. Results

3.1. Tumor dose for the virtual respiratory patient model

3.1.1. Effects of motion in LR direction on tumor dose

Table 4 shows the differences in the DVH indices of tumor in different phases caused by respiratory motion in LR direction in the range of 3–13 mm. Within the motion amplitude of 13 mm, the differences of the mean dose and $D_{95\%}$ of tumor, which is the dose received by 95% of the tumor volume, in various phases were all within 3%.

3.1.2. Effects of motion in AP direction on tumor dose

Table 5 shows the percentage differences of the mean dose and $D_{95\%}$ of tumors in different phases in the AP direction. The differences of DVH indices at different phases increased with greater respiratory motion amplitude. For the motion amplitude ranged from 5 mm to 21 mm in the AP direction, the differences of tumor mean dose and $D_{95\%}$ ranged from −13.8% to 15.8% and −15.4%–18.2%, respectively.

3.1.3. Effects of motion in SI direction on tumor dose

Table 6 presents the percentage differences of the tumor mean dose and $D_{95\%}$ in different phases in the SI direction. Moreover, great tumor motion amplitude resulted in great differences among the various phases. For the motion range of 5 mm–34 mm in the SI direction, the differences of tumor mean dose and $D_{95\%}$ ranged from −4.5% to 0.5% and 9.1%–2.8%, respectively.

Table 5
Percentage differences of mean dose and $D_{95\%}$ at different phases in the range of 5–21 mm in AP motion.

Phase	Dose	Tumor dose differences (%) at each phase of different motion amplitudes in the AP direction				
		5 mm	9 mm	13 mm	17 mm	21 mm
10%	D_{mean}	−0.4	2.6	2.6	5.8	5.8
	$D_{95\%}$	−0.6	3.2	3.2	6.7	6.7
20%	D_{mean}	–	–	–	–	–
	$D_{95\%}$	–	–	–	–	–
50%	D_{mean}	−2.4	−5.3	−8.2	−11.0	−13.8
	$D_{95\%}$	−3.5	−6.5	−9.7	−12.6	−15.4
60%	D_{mean}	−2.3	−5.1	−5.1	−7.9	−10.8
	$D_{95\%}$	−3.2	−6.3	−6.3	−9.5	−12.6
80%	D_{mean}	0.1	0.1	3.1	3.1	6.3
	$D_{95\%}$	0.4	0.2	3.7	3.7	7.4
90%	D_{mean}	2.5	5.7	9.0	12.4	15.8
	$D_{95\%}$	3.0	6.5	10.2	14.3	18.2

*Represents the percentage differences greater than 5%.

Table 6
Percentage differences of mean dose and $D_{95\%}$ at different phases in the range of 5–34 mm in SI motion.

Phase	Dose	Tumor dose differences (%) at each phase of different motion amplitudes in the SI direction				
		5 mm	12 mm	19 mm	26 mm	34 mm
10%	D_{mean}	−0.4	−0.2	−0.1	−0.1	−0.1
	$D_{95\%}$	−0.6	0.2	0.9	0.9	1.7
20%	D_{mean}	0	0	0	0	0
	$D_{95\%}$	0	0	0	0	0
50%	D_{mean}	0.2	−0.8	−1.4	−2.8	−4.5
	$D_{95\%}$	−0.9	−2.6	−3.7	−6.1	−9.1
60%	D_{mean}	0.4	−0.1	−0.6	−2.6	−3.4
	$D_{95\%}$	−0.4	−1.1	−2.8	−6.3	−7.6
80%	D_{mean}	0.1	0.3	0.5	0.5	0.5
	$D_{95\%}$	0.4	0.9	1.5	1.5	1.9
90%	D_{mean}	−0.3	−0.2	−0.3	−0.8	−1.7
	$D_{95\%}$	0.2	1.1	1.7	2.6	2.8

*Represents the percentage differences greater than 5%.

3.2. Effect of respiratory motion on the tumor dose in the real patient cases

3.2.1. Dose analysis of patient I

For Patient I, the ranges of the tumor motion in the three directions were all within 2 mm. In Fig. 4, the dose differences of tumors in various phases were within 2% and the percentage difference of tumor mean dose integrated over the respiratory cycle was −0.5% compared with the reference phase. The differences in the affected side lung were less than 5% among different phases. The maximum difference was observed at the 90% phase.

3.2.2. Dose analysis of patient II

For Patient II, the tumor motion ranged in the SI, LR, and AP directions were 10, 3, and 1.5 mm, respectively. Fig. 5 shows that the percentage differences of tumor mean dose and $D_{95\%}$ were all within 1.5% among different phases and the percentage difference of tumor mean dose integrated over the respiratory cycle was −0.4% compared with the reference phase. The differences of mean lung dose and V_5 of the lung in the affected side were within 3% compared with the reference phase.

3.2.3. Dose analysis of patient III

For Patient III, the tumor motion ranges of SI, LR, and AP directions were 16, 3 and 2 mm, respectively. Fig. 6 shows that the percentage difference of tumor mean dose and $D_{95\%}$ at the end-inhaled phase all reached to 9%, respectively. The percentage difference of tumor mean dose integrated over the respiratory cycle was −2.8% compared with the reference phase. The most significant difference of mean lung dose and V_5 of the lung in the affected side was more than 3% compared with the reference phase. The liver was directly exposed to the neutron beam, because the tumor was at the junction of the lower lobe and liver. Thus, absolute volume of V_0–$V_{9.1}$ at different phases was paid attention to. Although the relative difference of V_0–$V_{9.1}$ was large, the absolute value of V_0–$V_{9.1}$ at different phases were much lower than the volume limit.

4. Discussion

BNCT dose depends on both neutron flux and boron concentration. Due to respiratory motion, the neutron flux distribution of the places where the tumor located will be affected by changes in tumor location, which may impact the BNCT dose distribution in patient, thereby resulting in a lack of tumor dose in edge and lead to poor efficacy. Tumor recurrence may ensue. In previous studies, researchers explored the dosimetric impact of shifts in patient positioning during BNCT for brain tumors. Significant impacts (10%) were seen for longitudinal
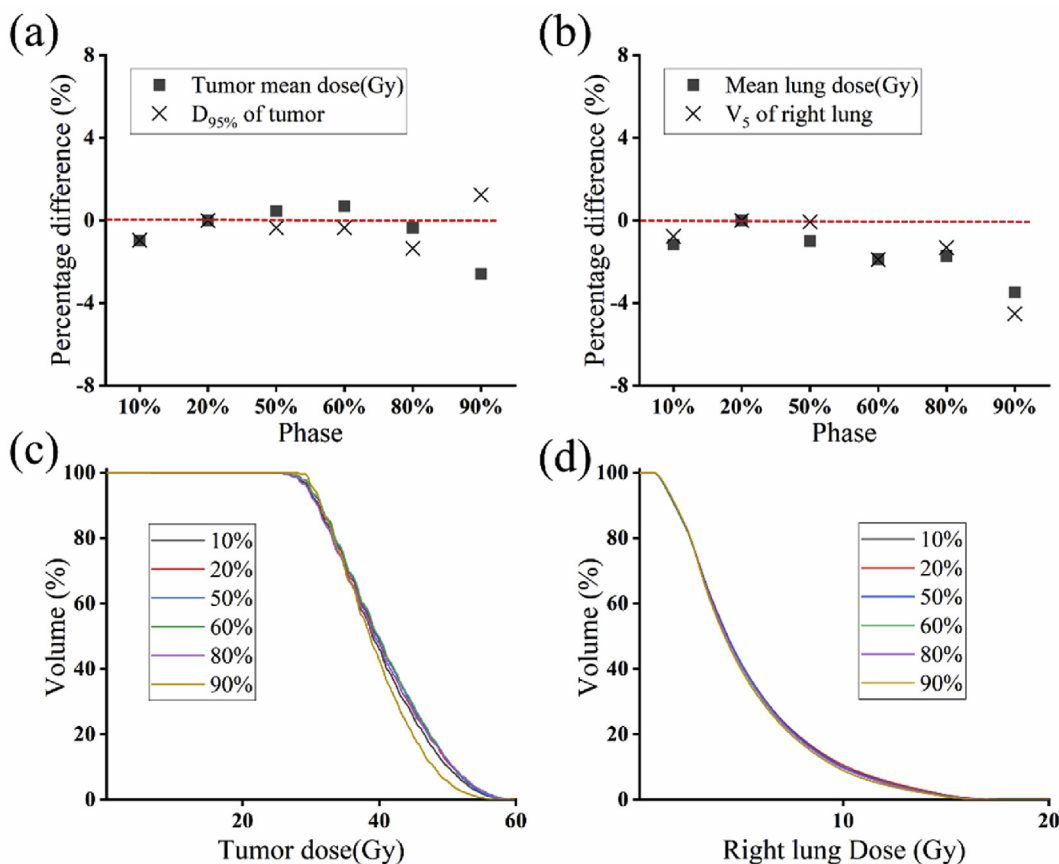
Fig. 4. (a) Percentage difference in the mean dose and $D_{95\%}$ of tumors at different phases; (b) Percentage difference in the mean dose and V_5 of the right lung at different phases; (c) DVH for tumor; and (d) DVH for right lung at six phases.

displacements of less than 1 cm (Takada et al., 2016). The dose affected by displacement at different depths was also investigated (Lee et al., 2018). The feasibility of BNCT in lung cancer treatment has been verified through dosimetric calculations and experiments. However, changes in the dose caused by respiratory motion have not been explored.

In order to verify the degree of accuracy of the results obtained in this study. The dose deviation results from the tumor movements with different amplitudes of motion were compared with the data in the previous report (Lee et al., 2018), in which mean tumor dose changes following shifts in the patient brain models were analyzed. The mean tumor dose differences of the virtual respiratory patient model listed here are the differences between the end-inhaled phase and the end-exhaled phase, because the tumor position differences between the two phases are 1, 2, and 3 cm. We compared the dose changes caused by tumor movement in the radial direction of the neutron beam (as listed in Table 7). The virtual respiratory patient model in this study had a tumor depth of 3.2 cm. The tumor extention in SI direction was 4.8 cm. The tumor volume was 17.5 cc. These were different from the parameters of the tumor in the previous study (i.e., tumor height was 5 cm, tumor volume was 35.4 cc). Thus, the dose differences at various shift distances were different, but all were on the same magnitude.

In this study, the mean tumor dose and $D_{95\%}$ of different phases increased with the increase of tumor motion amplitudes. In a previously study about motion range (Erridge et al., 2003), the movement in the LR direction (3–13 mm) had little effect on the tumor dose under the above treatment planning configurations. The dosimetry changes between different phases caused by tumor movement in the AP direction were obvious. The reason is that neutron source was irradiated from front to back of the human body. The movement of the tumor in the AP

direction was equivalent to the shifting of the tumor position along the axial direction of the neutron beam. The changes of flux density and energy of the neutron in the axial direction were more sensitive than those in the radial direction. Thus, the motion in the AP direction had a greater influence on the tumor dose than motion in other directions (Takada et al., 2016). But when integrating the tumor mean dose over the respiratory cycle, the maximal percentage difference was only 0.5% compared with the reference phase. In the range of motions from 5 to 34 mm at SI direction, when the tumor movement exceeded 20 mm, the differences of $D_{95\%}$ should receive particular attention. When integrating the tumor mean dose over the respiratory cycle, the maximal percentage difference was −1.5% compared with the reference phase. Therefore, the study of a virtual respiratory patient model found that within the range of respiratory movements that can be achieved, the tumor mean dose difference due to respiratory motion during the treatment of lung cancer with BNCT was within 2%.

Three patients with different motion ranges were investigated, and the obtained tumor mean dose were compared with the results of the virtual respiratory patient model to verify the applicability of the conclusions obtained from the aforementioned studies. For Patient I who had small tumor movement amplitude, the mean tumor dose differences among different phases were within 2%. The mean tumor dose's integrated difference among different phases was −0.5% compared to the reference phase, and the integrated difference of the virtual respiratory patient model with similar motion range (5 mm in SI direction and 3 mm in LR direction) was approximately −0.1%. For Patient II, the maximum difference of the mean tumor dose between different phases was within 1.5%, and the maximum difference of the virtual respiratory patient model with similar motion range (12 mm in SI direction and 3 mm in LR direction) was approximately 1.6%. The
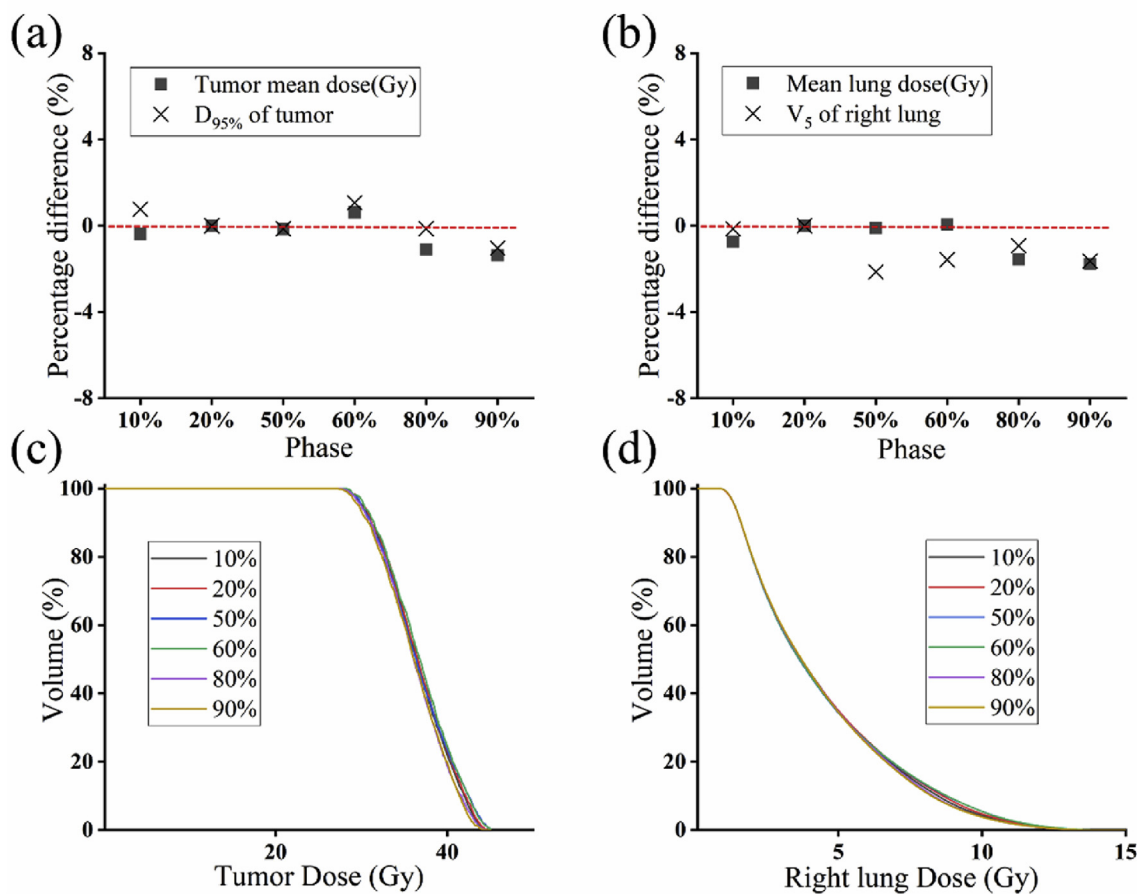
Fig. 5. (a) Percentage difference in the mean dose and $D_{95\%}$ of tumors at different phases; (b) Percentage difference in the mean dose and V_5 of the right lung at different phases; (c) DVH for tumor; and (d) DVH for right lung at six phases.
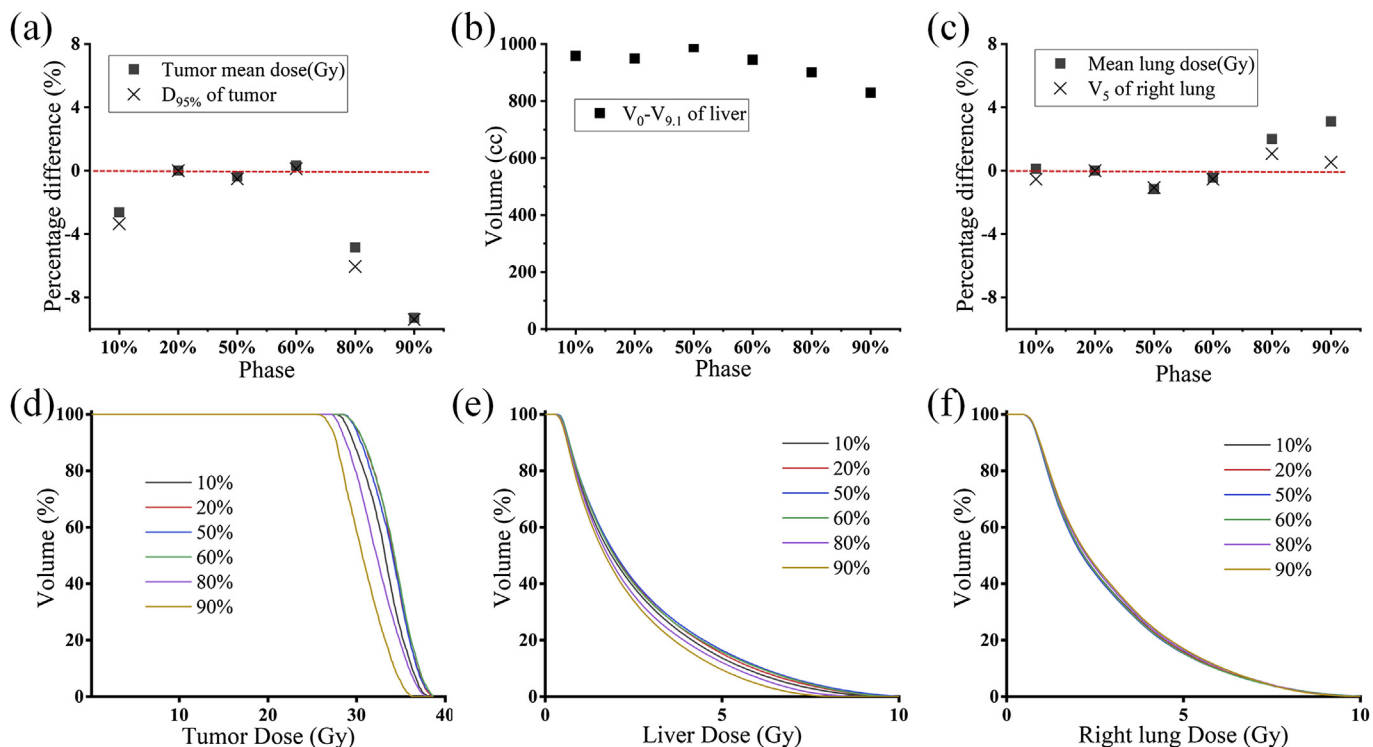
Fig. 6. (a) Percentage difference in the mean dose and $D_{95\%}$ of tumors at different phases; (b) Absolute volume of V_0–$V_{9.1}$ at different phases; (c) Percentage difference in the mean dose and V_5 of the right lung at different phases; (d) DVH for tumor; (e) DVH for liver; and (f) DVH for right lung at six phases.

Table 7

Percentage changes for mean tumor dose of the brain model at THOR and virtual respiratory patient model with lateral shifts of tumor parallel to the beam port.

Distance and type of shift	THOR (%)		Virtual respiratory patient model
	[a]$T_{6.5cm}$	[a]$T_{2.5cm}$	
1 cm lateral shift	1.4	0.6	0.5
2 cm lateral shift	5.5	3.6	1.9
3 cm lateral shift	11.1	8.8	5.0

[a] $T_{6.5cm}$ and $T_{2.5cm}$ indicate that the depth of the tumor center are 6.5 and 2.5 cm, respectively. In the study of THOR, the tumor was a virtual cylindrical brain tumor with a height of 5 cm and a basal diameter of 3 cm.

mean tumor dose's integrated difference among different phases was −0.4% compared to the reference phase. And the integrated difference of the virtual respiratory patient model with similar motion range was approximately −0.2%. The results were close. For Patient III, the mean tumor dose's maximum difference among different phases reached 9%, and the maximum difference of the virtual respiratory patient model with similar motion range (19 mm in the SI direction and 3 mm in the LR direction) was approximately 2.1%. The mean tumor dose's integrated difference among different phases was −2.8%, and for the virtual respiratory patient model, the integrated difference was approximately −0.4%. They differed to some extent. The reasons may be as follows. First, the real patient's tumor had a motion amplitude of 2 mm in the AP direction. In the virtual respiratory patient model, the difference caused by the tumor motion in the AP direction was not considered in the result estimation, because the motion amplitude of 2 mm was not set. Therefore, the two values differed. Second, the distinctions of tumor geometry and location may also result in differences between the two results. The virtual respiratory patient model is effective for predicting tumor dose differences caused by small-scale respiratory motion. But for patients with large-scale respiratory motion and due to differences in tumor parameters, the predicted value is smaller.

This study had several limitations. First, the impact of the respiratory motion when multiple portals are set was not evaluated, maybe the results are different in such a setting. Second, for the construction of the model with a small motion range, the voxel size in this study was not small enough (for example, for the motion range of 3 mm, the minimum difference in tumor position between different phases is less than 1 mm). Thus, the simulated tumor motion amplitude was not realistic.

5. Conclusion

The effects of respiratory motion with different motion directions and amplitudes on tumor DVH indices in treating lung cancer using BNCT were investigated. In the three movement directions, the motion in the orientation parallel to the irradiation direction (e.g. AP in the current study) had the greatest influence on the DVH indices. This finding proved that tumor movement affects tumor dose, the extent of the impact was within 5%. The results from the patient cases with small-scale respiratory motion were consistent with that from the virtual respiratory patient model.

Acknowledgements

References

Agostinelli, S., Allison, J., Amako, K., Apostolakis, J., Araujo, H., Arce, P., Asai, M., Axen, D., Banerjee, S., Barrand, G., 2003. GEANT4—a simulation toolkit. 2. Nucl. instruments methods Phys. Res. Sect. A Accel. Spectrometers, Detect. Assoc. Equip. 506, 250–303.

Allison, J., Amako, K., Apostolakis, J.E.A., Araujo, H., Dubois, P.A., Asai, M., Barrand, G., Capra, R., Chauvie, S., Chytracek, R., 2006. Geant4 developments and applications. IEEE Trans. Nucl. Sci. 53, 270–278.

Alvarado-Luna, G., Morales-Espinosa, D., 2016. Treatment for small cell lung cancer, where are we now?—a review. Transl. Lung Cancer Res. 5, 26.

Benedict, S.H., Yenice, K.M., Followill, D., Galvin, J.M., Hinson, W., Kavanagh, B., Keall, P., Lovelock, M., Meeks, S., Papiez, L., 2010. Stereotactic body radiation therapy: the report of AAPM Task Group 101. Med. Phys. 37, 4078–4101.

Bray, F., Ferlay, J., Soerjomataram, I., Siegel, R.L., Torre, L.A., Jemal, A., 2018. Global cancer statistics 2018: GLOBOCAN estimates of incidence and mortality worldwide for 36 cancers in 185 countries. CA A Cancer J. Clin. 68, 394–424.

Eom, J., Xu, X.G., De, S., Shi, C., 2010. Predictive modeling of lung motion over the entire respiratory cycle using measured pressure-volume data, 4DCT images, and finite-element analysis. Med. Phys. 37, 4389–4400.

Erridge, S.C., Seppenwoolde, Y., Muller, S.H., van Herk, M., De Jaeger, K., Belderbos, J.S.A., Boersma, L.J., Lebesque, J.V., 2003. Portal imaging to assess set-up errors, tumor motion and tumor shrinkage during conformal radiotherapy of non-small cell lung cancer. Radiother. Oncol. 66, 75–85.

Ettinger, D.S., Wood, D.E., Aisner, D.L., Akerley, W., Bauman, J., Chirieac, L.R., D'Amico, T.A., DeCamp, M.M., Dilling, T.J., Dobelbower, M., 2017. Non–small cell lung cancer, version 5.2017, NCCN clinical practice guidelines in oncology. J. Natl. Compr. Cancer Netw. 15, 504–535.

Farías, R.O., Bortolussi, S., Menéndez, P.R., González, S.J., 2014. Exploring boron neutron capture therapy for non-small cell lung cancer. Phys. Med. 30, 888–897.

Geng, C., Tang, X., Guan, F., Johns, J., Vasudevan, L., Gong, C., Shu, D., Chen, D., 2015. GEANT4 calculations of neutron dose in radiation protection using a homogeneous phantom and a Chinese hybrid male phantom. Radiat. Prot. Dosim. 168, 433–440.

George, R., Vedam, S.S., Chung, T.D., Ramakrishnan, V., Keall, P.J., 2005. The application of the sinusoidal model to lung cancer patient respiratory motion. Med. Phys. 32, 2850–2861.

González, S.J., Bonomi, M.R., Santa Cruz, G.A., Blaumann, H.R., Larrieu, O.A.C., Menéndez, P., Rebagliati, R.J., Longhino, J., Feld, D.B., Dagrosa, M.A., 2004. First BNCT treatment of a skin melanoma in Argentina: dosimetric analysis and clinical outcome. Appl. Radiat. Isot. 61, 1101–1105.

Grassberger, C., Dowdell, S., Lomax, A., Sharp, G., Shackleford, J., Choi, N., Willers, H., Paganetti, H., 2013. Motion interplay as a function of patient parameters and spot size in spot scanning proton therapy for lung cancer. Int. J. Radiat. Oncol. Biol. Phys. 86, 380–386.

Ishiyama, S., 2014. Deterministic parsing model of the compound biological effectiveness (CBE) factor for intracellular 10Boron distribution in boron neutron capture therapy. J. Cancer Ther. 5, 1388.

Kiger III, W.S., Sakamoto, S., Harling, O.K., 1999. Neutronic design of a fission converter-based epithermal neutron beam for neutron capture therapy. Nucl. Sci. Eng. 131, 1–22.

Knopf, A.-C., Hong, T.S., Lomax, A., 2011. Scanned proton radiotherapy for mobile targets—the effectiveness of re-scanning in the context of different treatment planning approaches and for different motion characteristics. Phys. Med. Biol. 56, 7257.

Lee, J.-C., Chen, Y.-W., Chuang, K.-S., Hsu, F.-Y., Chou, F.-I., Hsu, S.-M., Yen, S.-H., Wu, Y.-H., 2018. The dosimetric impact of shifts in patient positioning during boron neutron capture therapy for brain tumors. BioMed Res. Int. 2018, 1–11 2018.

Leunens, G., Verstraete, J., Dutreix, A., Van der Schueren, E., 1992. Assessment of dose inhomogeneity at target level by in vivo dosimetry: can the recommended 5% accuracy in the dose delivered to the target volume be fulfilled in daily practice? Radiother. Oncol. 25, 242–250.

Moss, R.L., 2014. Critical review, with an optimistic outlook, on boron neutron capture therapy (BNCT). Appl. Radiat. Isot. 88, 2–11.

Perl, J., Shin, J., Schümann, J., Faddegon, B., Paganetti, H., 2012. TOPAS: an innovative proton Monte Carlo platform for research and clinical applications. Med. Phys. 39, 6818–6837.

Schaefer, M., Münter, M.W., Thilmann, C., Sterzing, F., Haering, P., Combs, S.E., Debus, J., 2004. Influence of intra-fractional breathing movement in step-and-shoot IMRT. Phys. Med. Biol. 49, N175.

Schneider, W., Bortfeld, T., Schlegel, W., 2000. Correlation between CT numbers and tissue parameters needed for Monte Carlo simulations of clinical dose distributions. Phys. Med. Biol. 45, 459.

Suzuki, M., Sakurai, Y., Masunaga, S., Kinashi, Y., Nagata, K., Maruhashi, A., Ono, K., 2006. Feasibility of boron neutron capture therapy (BNCT) for malignant pleural mesothelioma from a viewpoint of dose distribution analysis. Int. J. Radiat. Oncol. Biol. Phys. 66, 1584–1589.

Suzuki, M., Suzuki, O., Sakurai, Y., Tanaka, H., Kondo, N., Kinashi, Y., Masunaga, S., Maruhashi, A., Ono, K., 2012. Reirradiation for locally recurrent lung cancer in the chest wall with boron neutron capture therapy (BNCT). In: International Cancer Conference Journal. Springer, pp. 235–238.

Takada, K., Kumada, H., Liem, P.H., Sakurai, H., Sakae, T., 2016. Development of Monte Carlo based real-time treatment planning system with fast calculation algorithm for boron neutron capture therapy. Phys. Med. 32, 1846–1851.

Yang, S.-N., Lin, C.-W., Chang, M.-B., Zhang, G.G., Chou, K.-T., Chiou, Y.-R., Sun, S.-S., Lui, L., Ho, T.-J., Huang, T.-C., 2018. Dose verification for tumor motion with different treatment planning systems: a dynamic thorax phantom study. J. Med. Biol. Eng. 38, 46–54.

Yu, H., Tang, X., Shu, D., Liu, Y., Geng, C., Gong, C., Hang, S., Chen, D., 2017. Influence of neutron sources and 10B concentration on boron neutron capture therapy for shallow and deeper non-small cell lung cancer. Health Phys. 112, 258–265.